INTERFEROMETRY BY MULTIDIMENSIONAL DECONVOLUTION FOR TIME-LAPSE CONTROLLED SOURCE ELECTROMAGNETICS

*J. Hunziker, E. Slob and K. Wapenaar**

Delft University of Technology
Department of Geotechnology
Stevinweg 1, 2628 CN Delft, The Netherlands

ABSTRACT

Time-lapse marine Controlled Source Electromagnetics is capable of detecting changes in a subsurface reservoir. However, changes related to the source or the ocean affect the data much more than possible changes in a reservoir. We show that those unwanted effects can be largely suppressed by applying interferometry by multidimensional deconvolution. Two numerical examples illustrate that the resulting reflection response contains only effects related to the subsurface.

***Index Terms*—** Controlled Source Electromagnetics, Exploration, Interferometry, Time-lapse

1. INTRODUCTION

Subsurface exploration with seismic methods is able to delineate geologic structures, but it is not able to distinguish between a structure whose porous rock is water filled and another structure that is filled with hydrocarbons. Since hydrocarbons have a much higher electric resistivity than water, they can be detected by electric methods. Therefore, it is useful to conduct a marine Controlled Source Electromagnetics (CSEM) survey, in addition to a seismic survey, in order to determine if the structures located by seismics bear hydrocarbons or not. In frequency-domain marine CSEM an electric source is towed by a boat over a set of multicomponent receivers at the ocean bottom. The source emits continuously a monochromatic low-frequency signal. A part of the resulting electric field is diffusing through the subsurface, samples possible resistors and is finally recorded at the receivers. For a more detailed introduction to CSEM see [1].

In this study, we focus on time-lapse CSEM measurements for reservoir monitoring. [2] have shown that CSEM is sensitive to changes in thickness of a subsurface resistor, which hints at the feasibility of time-lapse CSEM. It was shown numerically, that changes in the reservoir response are measurable if the maximum repeatability error of the CSEM measurement is less than 1% to 2% [3, 4]. To achieve such a repeatability of the measurement, we propose to use interferometry by multidimensional deconvolution (MDD). Interferometry redatums arbitrarily distributed sources with random source strengths to a well-defined receiver array. In other words, it does not matter, where the sources are located in the ocean and therefore source-mispositioning issues become irrelevant. Furthermore, it replaces the overburden, i.e. everything above the receivers, with a homogeneous halfspace. Therefore, possible changes in seawater conductivity are removed as well and, generally, the detectability of changes in the subsurface is increased, because effects related to the air-water interface are removed. The only possibly problematic issue that remains in time-lapse CSEM is the repeatability of the receiver positions, but that should be easier to achieve than the repeatability of the source, because the receivers are stationary.

*This research is supported by the Dutch Technology Foundation STW, applied science division of NWO and the Technology Program of the Ministry of Economic Affairs.

2. THEORY

Interferometry by MDD can be divided into two parts: First, the recorded electromagnetic fields need to be decomposed into upward and downward decaying components, which was first done by [5]. We use an algorithm of [6], which in 3D needs all four horizontal components of the electromagnetic field. In this study, we use 2D transverse magnetic data, which means, that the source is infinitely long in the second spatial direction ($y-$direction). In this case, the decomposition can be done with just two components, the inline electric component E_x and the crossline magnetic component H_y. To perform the decomposition, the material parameters just below the ocean bottom, but not those of the ocean, are necessary. In the space-frequency domain, the upward decaying field $\hat{P}^-(x_R, x_S)$ is related with the downward decaying field $\hat{P}^+(x'_R, x_S)$ through the reflection response $\hat{R}_0^+(x_R, x'_R)$

$$\hat{P}^-(x_R, x_S) = \int_{\partial D_R} \hat{R}_0^+(x_R, x'_R)\hat{P}^+(x'_R, x_S)dx'_R, \quad (1)$$

where x_R and x'_R are the coordinates of receiver stations, whereas x_S is the source position. The circumflex denotes the space-frequency domain. The superscript $^+$ in the reflection

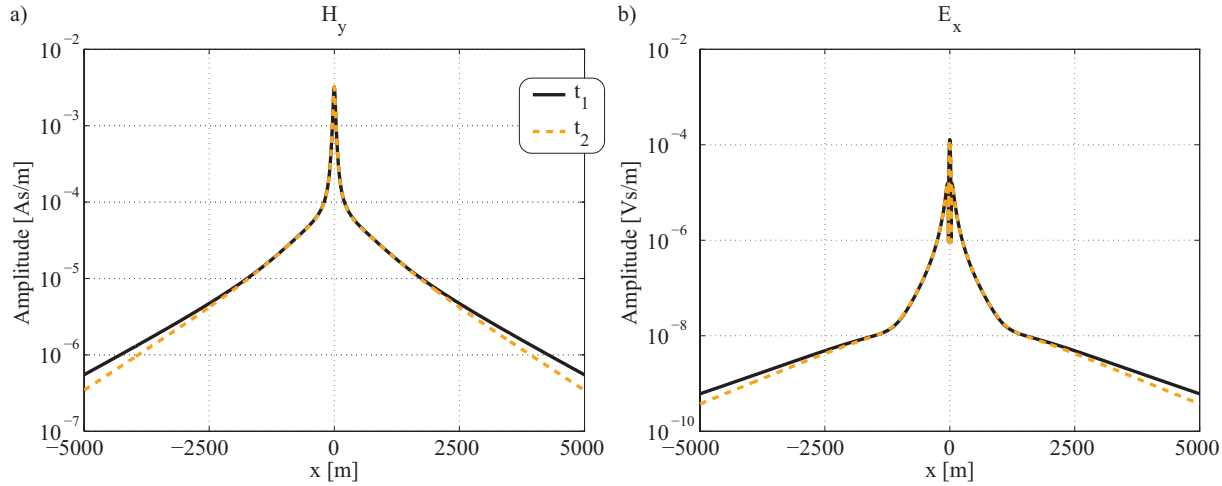

Fig. 1. a) The crossline magnetic field H_y and b) the inline electric field E_x recorded at the first time of measurement t_1 (solid black curve) and at the second time of measurement t_2 (dashed orange curve) as a function of offset with respect to the source position. Note that the amplitude scale is different for the electric field as for the magnetic field.

response indicates that its origin is a downward decaying field and the subscript $_0$ represents the absence of heterogeneities above the receiver level. This equation can be rewritten in matrix notation as described by [7] as

$$\hat{\mathbf{P}}^- = \hat{\mathbf{R}}_0^+ \hat{\mathbf{P}}^+. \tag{2}$$

Each column of the matrices contains various receiver positions for a fixed source position, while for the rows the situation is reversed.

In the second part, we solve equation 2 for the reflection response $\hat{\mathbf{R}}_0^+$, i.e. the scattered Green's function of the subsurface, by multidimensional deconvolution of the upward decaying field with the downward decaying field [8]. This can for example be achieved with a least-squares inversion:

$$\hat{\mathbf{R}}_\mathbf{0}^+ = \hat{\mathbf{P}}^- \left(\hat{\mathbf{P}}^+\right)^\dagger \left[\hat{\mathbf{P}}^+ \left(\hat{\mathbf{P}}^+\right)^\dagger + \varepsilon^2 \mathbf{I}\right]^{-1}. \tag{3}$$

The superscript † denotes complex-conjugation and transposition and $\mathbf{I}$ is the identity matrix. The stabilization parameter ε prevents the inversion from getting unstable.

In time-lapse CSEM, we apply interferometry by MDD to data recorded at all times of measurement in order to remove changes related to source position or salinity of the ocean. Then the retrieved subsurface reflection responses of two different times of measurement are compared. This is shown with two numerical examples in the next section.

3. RESULTS

We model electromagnetic fields due to a unit source at two different times for a layered Earth model containing a reservoir of 50 m thickness 1000 m below the ocean bottom. In the first time of measurement t_1, before production, the reservoir layer has a conductivity of 0.01 S/m, whereas the surrounding rock has a conductivity of 0.5 S/m. We consider two different scenarios of oil production.

3.1. Scenario 1

In the first scenario, the oil content is reduced homogeneously throughout the complete reservoir. To compute the conductivity of the reservoir layer after partial production, we use Archie's law [9], which relates the electric conductivity of a porous rock σ_r with its porosity ϕ and brine saturation S

$$\sigma_r = \sigma_b \left(\phi S\right)^2, \tag{4}$$

where σ_b is the conductivity of the brine (6.25 S/m). Assuming a porosity of 28% and, after production, a brine saturation of 20%, i.e. 20% of the oil has been produced, the electric conductivity of the reservoir layer is in the second time of measurement t_2 0.02 S/m. A third dataset is recorded at the same time, but with the source towed higher than at t_1 and t_2. We refer to this dataset as $t_{2,\text{error}}$. Random noise was added to the electric data at a level of 10^{-14} Vs/m and to the magnetic data at a level of 10^{-11} As/m. These noise levels are one magnitude larger than the noise floor of common CSEM measurements [10]. The inline electric component E_x and the crossline magnetic component H_y are shown for the two times of measurement t_1 and t_2 in Figure 1.

The electromagnetic fields at the two times of measurement are very similar. A subtraction of the fields at t_2 from those at t_1 reveals the differences more clearly. Figure 2a and 2b show the difference between t_1 and t_2 (solid red curve) and the difference between t_1 and $t_{2,\text{error}}$ (dashed blue curve), i.e. the difference between the measurement before production and the second measurement including the altered source

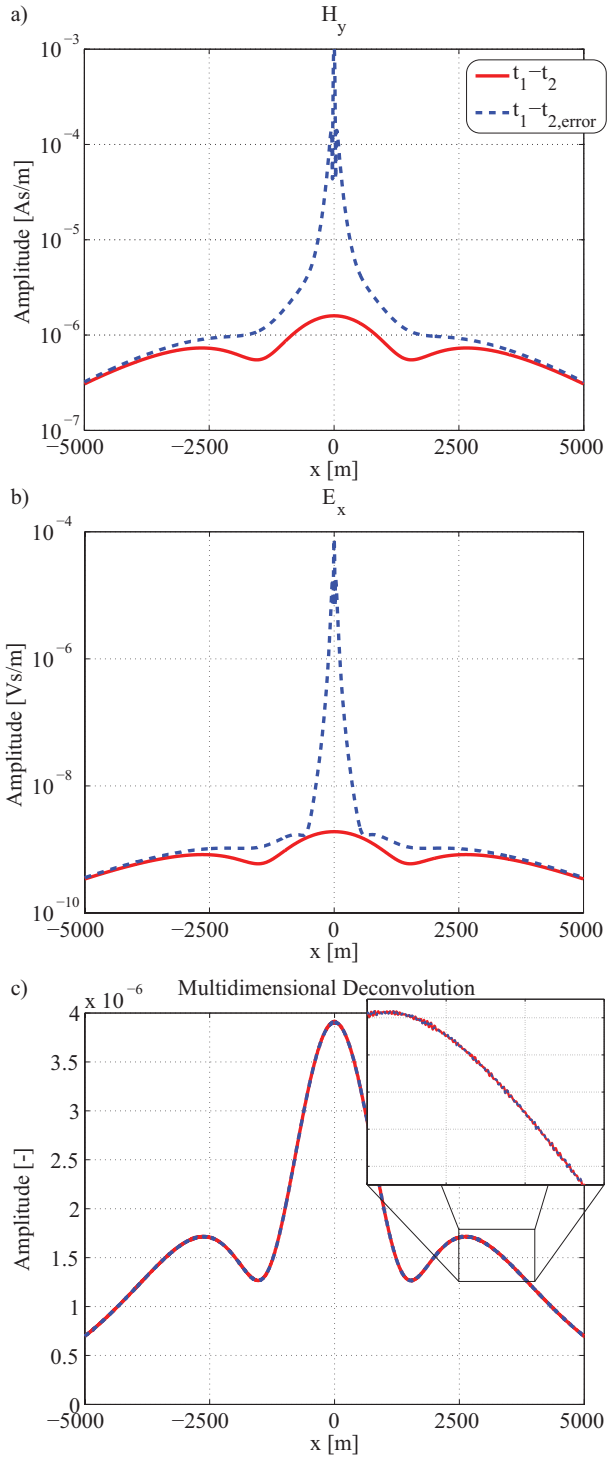

Fig. 2. Difference between two times of measurement: a) magnetic field in crossline direction, b) electric field in inline direction and c) retrieved reflection response. Solid red curve: $t_1 - t_2$; Dashed blue curve: $t_1 - t_{2,\text{error}}$. The inset of c) magnifies the area between 2500 and 4000 m offset and an amplitude range of $1.25 \cdot 10^{-6}$ and $1.75 \cdot 10^{-6}$.

position. The amplitude of the dashed blue curve is at small and intermediate offsets much larger than the one of the solid red curve. This means that the misplacement of the source has a larger impact on the recorded electromagnetic fields than the change of the conductivity of the reservoir layer from 0.01 S/m to 0.02 S/m.

We apply interferometry by MDD to these three datasets in order to redatum the source. The differences of the retrieved reflection responses are depicted in Figure 2c. Since interferometry redatums the source to receiver positions, the effect of the mispositioning of the source is removed. Therefore, the solid red curve ($t_1 - t_2$) is identical with the dashed blue curve ($t_1 - t_{2,\text{error}}$). This is achieved without knowing the actual source location in both time-lapse measurements. The inset of Figure 2c magnifies the reflection response between 2500 m and 4000 m offset. It can be seen, that the retrieved curve is slightly affected by the added noise.

3.2. Scenario 2

In the second scenario also 20% of the oil is produced, but in this scenario the lowest part of the reservoir is swepted completely, whereas there is no change in oil content in the upper part. This bottom flodding scenario is modeled by using a 20% thinner reservoir. Similar to the first scenario, we consider a time of measurement before production t_1 and a second time of measurement during production t_2. Additionally, we also model a dataset $t_{2,\text{error}}$ with a different salinity of the ocean. This is simulated by changing the conductivity of the water layer from 3 S/m to 3.2 S/m. The source is in all three datasets at the same position.

Figure 3a and 3b show the difference between the datasets during and before production. A comparison of the dashed blue curve ($t_1 - t_{2,\text{error}}$) with the solid red curve ($t_1 - t_2$) indicates, that the effect of the changed ocean salinity has a more significant impact on the data than the change in the reservoir thickness. This is especially at small and intermediate offsets the case. Also this effect can be removed by applying interferometry by MDD (Figure 3c). To achieve this, the conductivity of the ocean does not need to be known. Only the conductivity just below the ocean bottom is required for the decomposition, which can be easily obtained from local measurements.

4. CONCLUSIONS

Changes in the reservoir (thickness or conductivity) are detectable with CSEM, but an altered source position or ocean salinity have a much larger impact on the data. By applying interferometry by MDD, the medium above the receivers is replaced by a homogeneous halfspace and the sources are redatumed to receiver positions. Consequently, effects related to the source or the overburden can be largely suppressed. The difference between reflection responses retrieved by MDD

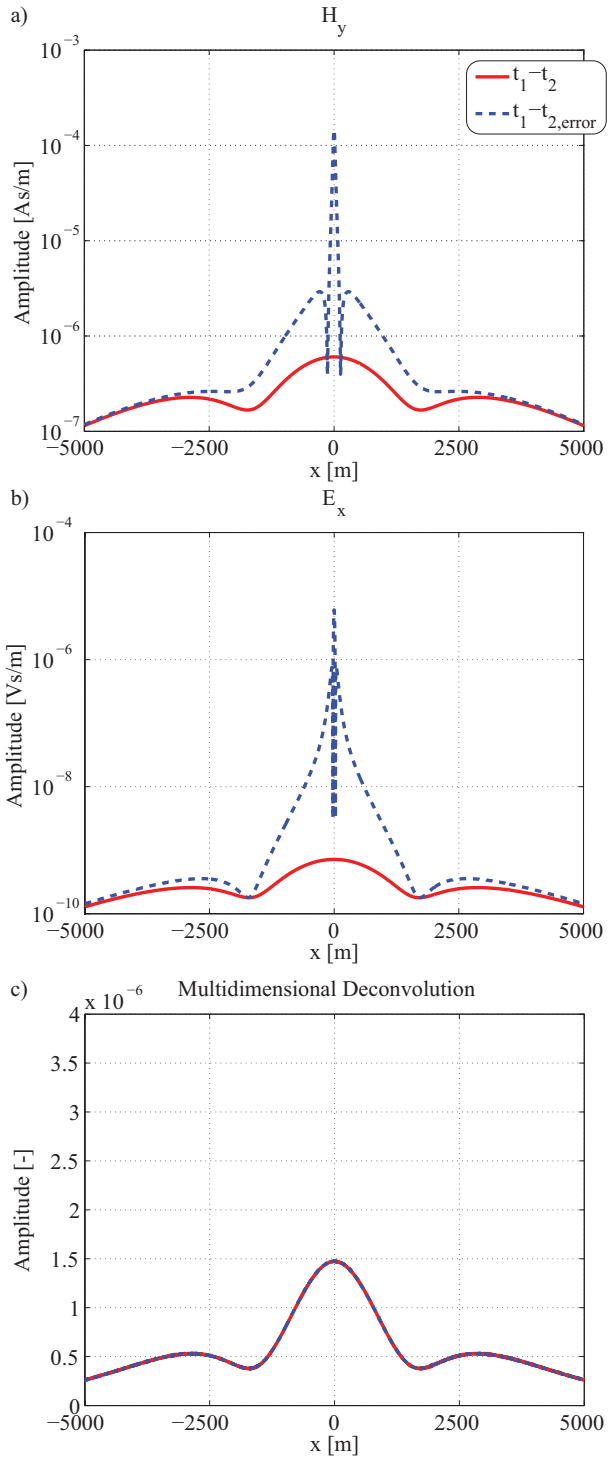

Fig. 3. Same as Figure 2 for the second scenario.

before production and during production is only affected by changes in the subsurface.

A comparison of Figures 2c and 3c shows that a thinning of the reservoir (scenario 2) alters the subsurface response less than changes of the conductivity throughout the whole reservoir (scenario 1). Still, both are detectable even with a noise floor of one order of magnitude larger than for common CSEM measurements.

5. REFERENCES

[1] S. Constable and L. J. Srnka, "An introduction to marine controlled-source electromagnetic methods for hydrocarbon exploration," *Geophysics*, vol. 72, pp. WA3–WA12, 2007.

[2] S. Constable and C. J. Weiss, "Mapping thin resistors and hydrocarbons with marine EM methods: Insights from 1D modeling," *Geophysics*, vol. 71, pp. G43–G51, 2006.

[3] A. Orange, K. Kerry, and S. Constable, "The feasibility of reservoir monitoring using time-lapse marine csem," *Geophysics*, vol. 74, pp. F21–F29, 2009.

[4] M. Wirianto, W. A. Mulder, and E. C. Slob, "A feasibility study of land CSEM reservoir monitoring in a complex 3-D model," *Geophysical Journal International*, vol. 181, pp. 741–755, 2010.

[5] L. Amundsen, L. Løseth, R. Mittet, S. Ellingsrud, and B. Ursin, "Decomposition of electromagnetic fields into upgoing and downgoing components," *Geophysics*, vol. 71, pp. G211–G223, 2006.

[6] E. Slob, "Interferometry by deconvolution of multicomponent multioffset GPR data," *IEEE Transactions on Geoscience and Remote Sensing*, vol. 47, pp. 828–838, 2009.

[7] A. J. Berkhout, *Seismic Migration. Imaging of Acoustic Energy by Wave Field Extrapolation*, Elsevier, 1982.

[8] K. Wapenaar, E. Slob, and R. Snieder, "Seismic and electromagnetic controlled-source interferometry in dissipative media," *Geophysical Prospecting*, vol. 56, pp. 419–434, 2008.

[9] G. E. Archie, "The electrical resistivity log as an aid in determining some reservoir characteristics," *Petroleum Transactions, AIME*, vol. 146, pp. 54–62, 1942.

[10] S. Constable, "Ten years of marine CSEM for hydrocarbon exploration," *Geophysics*, vol. 75, pp. 75A67–75A81, 2010.